THE ASTROPHYSICAL JOURNAL, 458:172–177, 1996 February 10

COMPLEX GASEOUS STRUCTURE IN THE NUCLEUS OF NGC 5252[1]

ZLATAN I. TSVETANOV,[2] JON A. MORSE,[3] ANDREW S. WILSON,[3,4] AND GERALD CECIL[5]
Received 1995 June 28; accepted 1995 August 16

ABSTRACT

We present several *Hubble Space Telescope* (*HST*) WFPC2 emission-line and continuum images of NGC 5252, a Seyfert 2 S0 galaxy with a large-scale "ionization bi-cone." In the Hα + [N II] image, the nucleus is bracketed at ∼0.″3 radii by two bright emission-line clumps along P.A. = 35° (∼20° from the major axis of the large-scale stellar disk). These three knots dominate the emission in the innermost ∼1″ (∼450 pc at 92 Mpc distance). Two major and several smaller spiral filaments, wound tightly counterclockwise, extend ∼3″ to the northwest and ∼4.″5 to the southeast of the nucleus. Several of these filaments extend from the two clumps near the nucleus, possibly indicating that the three collinear knots comprise a bar. Our Fabry-Perot velocity map shows that the spiral pattern is rotating, in a disk inclined significantly to both the galaxy stellar disk and the radio jets. The nuclear radio jets appear to have no obvious association with the Hα + [N II] filaments and clumps. Although most of the line flux is emitted within the inward extrapolation of the large-scale ionization bi-cone, some of the Hα + [N II] filaments extend beyond the cone boundaries. A remarkable D-shaped pattern of obscuring dust is visible on the northwest side of the galaxy major axis. Most of the spiral filaments in the Hα + [N II] image also appear in the obscuration map. The extinction by the filaments requires a column density of $N_H \approx 5 \times 10^{20}$ cm^{-2}. If the filaments are uniformly filled, both the gas responsible for the extinction and the ionized gas responsible for the emission have number densities of a few cm^{-3}.

Subject headings: galaxies: individual (NGC 5252) — galaxies: ISM — galaxies: nuclei — galaxies: peculiar — galaxies: Seyfert

1. INTRODUCTION

It is well established that anisotropy in the escaping ionizing radiation plays an important role in active galactic nuclei (AGNs). In the unified model of AGNs (reviewed recently by Antonucci 1993), an optically thick torus surrounds the nuclear engine and broad-line region (BLR). Intrinsically similar objects will then differ in appearance depending on the orientation of the torus to the observer's line of sight. In particular, Seyfert 1 galaxies are viewed from within the opening angle of the torus, but in Seyfert 2 galaxies our line of sight to the nuclear continuum source and BLR is blocked by the torus.

The Seyfert 2 galaxy NGC 5252 provides strong support for the unified model. Ground-based [O III] λ5007 and Hα + [N II] images (Tadhunter & Tsvetanov 1989, hereafter TT89) reveal a sharply defined bi-cone that extends in a series of arcs out to a radius of ∼45″–50″ (a projected distance of ∼20 kpc) north and south of the nucleus. The bi-cone may result from shadowing of the ionizing radiation by an optically thick torus. In contrast, the continuum image shows a typical S0 galaxy. The major axis of the S0 disk is misaligned with the axis of the bi-cone by ∼30°. The observed opening angle of the bi-cone is 74° ± 2°, and its axis is at P.A. = 163° ± 2°.

Neutral hydrogen has been detected outside the bi-cone (Prieto & Freudling 1993), supporting the interpretation (TT89) of the emission-line shells as ionized sectors of continuous structures that surround the galaxy. Very Large Array images (Wilson & Tsvetanov 1994, hereafter WT94) show two weak jets that extend ∼2″ (1 kpc) on each side of the nuclear core source. The jets lie along the axis of the much larger bi-cone, as is the case in all other Seyfert galaxies with well-defined radio ejecta and ionization cones.

Recently published spectra of NGC 5252 (Osterbrock & Martel 1993; Acosta-Pulido et al. 1995) reveal a broad component in the nuclear Hα profile, resulting in reclassification as a Seyfert 1.9 galaxy. The emission-line ratios in the ionization bi-cone are consistent with photoionization by an AGN-like continuum (Acosta-Pulido et al. 1995). Contributions from additional sources of excitation, such as shocks, are possible close to the nucleus. The kinematics of the line-emitting gas are complex and differ from the stellar rotation curve (Held, Capaccioli, & Cappellaro 1992). Finally, Kotilainen & Prieto (1995, hereafter KP95) suggest from near-infrared images that the nucleus is heavily obscured. They also find a red feature (which may represent dust extinction) that extends perpendicular to the axis of the ionization cone.

In this paper we present the first *HST* images of NGC 5252, obtained after the successful refurbishment mission. These images reveal remarkable morphologies of both the line-emitting gas and the obscuring dust in the central region. Observations and data reductions are described in § 2, and results are discussed in § 3. The heliocentric recession velocity

[1] Based on observations with the NASA/ESA *Hubble Space Telescope*, obtained at the Space Telescope Science Institute, which is operated by the Association of Universities for Research in Astronomy, Inc., under NASA contract NAS 5-26555.

[2] Department of Physics and Astronomy, Johns Hopkins University, Baltimore, MD 21218; zlatan@pha.jhu.edu.

[3] Space Telescope Science Institute, 3700 San Martin Drive, Baltimore, MD 21218; morsey@stsci.edu.

[4] Astronomy Department, University of Maryland, College Park, MD 20742; wilson@astro.umd.edu.

[5] Department of Physics and Astronomy, University of North Carolina, Chapel Hill, NC 27599-3255; cecil@wrath.physics.unc.edu.

of NGC 5252 is $cz_{\rm helio} = 6926 \pm 28$ km s^{-1} (Huchra & Burg 1992), leading to a distance of 92 Mpc ($H_0 = 75$ km s^{-1} Mpc^{-1}) and a scale $1'' = 450$ pc.

2. WFPC2 IMAGING AND DATA REDUCTION

The data presented here were obtained with the Wide Field and Planetary Camera 2 of *HST* on 1994 May 9. NGC 5252 was imaged through narrow- and broadband filters to isolate several emission lines and a line-free continuum band. In Table 1 we list the filter, its mean wavelength and width, the chip where the nucleus was imaged, total integration time, signal-to-noise ratio (S/N) achieved near the nucleus (averaged in the central 10 × 10 pixels), and the major contributing line in the spectral region.

The images were reduced with the IRAF/STSDAS[6] software package. Standard WFPC2 pipeline files and procedures were used for the first three reduction steps: bad pixel masking, A/D correction, and bias subtraction. Then we performed the following reduction steps, as recommended by the WFPC2 instrument team (Holtzman et al. 1995a). The closest on-orbit "superbias" frame was scaled and subtracted to correct for the remaining low-level bias structure. A high S/N "superdark" image was scaled and subtracted to correct pixels that have constant dark rate. Pixels with significantly different or variable dark rate ("hot pixels") were adjusted by subtracting a so-called delta dark image (the difference between the superdark and the dark frame nearest in time to our observations). To correct for the pixel-to-pixel response and variations in the illumination, we applied the latest available flat fields for each filter and CCD chip.

We found no shifts between the images in each filter, although the images contained few stars with which to register. We used the STSDAS task "crrej" to average together frames taken through each filter, cleaning cosmic rays with 5 σ and 4 σ rejection iterations and 3 σ rejection for neighbors. Because the "crrej" task does not automatically weight the images by exposure time, each of the F336W and FQUVN images was first scaled to an exposure of 900 s before combining. This scaling adjusts only the mean level, so the noise in the scaled exposure will be underestimated by the model. To account for this, we increased the noise by 10% before combining the F336W and FQUVN exposures.

The continuum image was then scaled and subtracted from each of the on-band frames to form "pure" emission-line maps. Because our F588N continuum image was taken with the nucleus placed on a different chip to those used for the other filters, this image was rotated and aligned with each of the on-band images. The relative chip rotations and pixel scales are given in Holtzman et al. (1995a). For example, in the F673N image the nucleus was placed on PC1. The F588N frame was, therefore, rotated 89.48 counterclockwise and resampled to match the F673N pixel scale. The central peak of the continuum image was aligned with the peak in the Hα + [N II] on-band image. (We discuss the alignment of the optical continuum, the emission line, and radio continuum peaks in more detail below.) The aligned continuum image was first scaled in intensity by the ratios of the exposure times and filter efficiencies, plus a color term to account for the differences in wavelength. Then, the result was subtracted from the Hα + [N II] image. Images in [O II] λ3727 and [Ne V] $\lambda\lambda$3346, 3426 were formed in the same way. Variations in continuum color over the galaxy could introduce errors into the continuum-subtracted images, especially [Ne V] $\lambda\lambda$3346, 3426 and [O II] λ3727, but the magnitude of such errors is hard to assess. The effects of WFPC2 field distortions when rotating and aligning the continuum image were estimated to be insignificant and ignored.

Finally, the emission-line maps were flux calibrated by multiplying by the system throughput (Holtzman et al. 1995b) at the appropriate wavelength (following the methods described in Heathcote et al. 1995). To assess the accuracy of the flux calibration, we have compared emission-line fluxes derived from the WFPC2 observations and the ground-based images of TT89 obtained in nearly photometric conditions. The contribution of the [N II] $\lambda\lambda$6548, 6583 lines to each Hα + [N II] image was estimated by accounting for the filter transmission at the redshifted line wavelengths. We estimate that $F(\text{H}\alpha + [\text{N II}])_{\rm WFPC2} = F(\text{H}\alpha)(1.22\Re + 1)$ and $F(\text{H}\alpha + [\text{N II}])_{\rm TT89} = F(\text{H}\alpha)(0.58\Re + 1)$, where $\Re = [\text{N II}]\ \lambda6583/\text{H}\alpha$. Ground-based spectra (Acosta-Pulido et al. 1995) indicate that $\Re \sim 0.5$ throughout the nuclear region. Under these assumptions, the total Hα flux within an aperture of 9.1 centered on the nucleus as measured from the *HST* image is found to agree to within 5% with the flux measured from the ground-based image of TT89. We estimate the overall calibration of the WFPC2 emission-line fluxes to be accurate to ~5%–10%.

3. RESULTS AND DISCUSSION

3.1. *Morphology of the Line-emitting Gas*

The continuum-subtracted Hα + [N II] map of NGC 5252 is shown in Figure 1*a*, where we have adjusted the contrast to emphasize faint emission in the arcs away from the nucleus. In this figure, the outer parts of the WFPC2 field of view are excluded because we detected no structure in these areas. Figure 2*a* (Plate 4) shows the innermost 11″ of the Hα + [N II] image at full resolution. The other two line emission

[6] The Image Reduction and Analysis Facility (IRAF) is distributed by the National Optical Astronomy Observatories, which is operated by the Association of Universities for Research in Astronomy, Inc., under contract to the National Science Foundation. The Space Telescope Science Data Analysis System (STSDAS) is distributed by the Space Telescope Science Institute.

TABLE 1

OBSERVING LOG

Filter	$\lambda_c/\Delta\lambda$ (Å)	WFPC2 Chip	$t_{\rm exp}$ (s)	S/N Ratio	Wavelength Coverage
F673N	6733/47	PC1	2 × 900	175	Hα + [N II]
F588N	5893/49	WF2	2 × 1200	150	Continuum
FQUVN.....	3830/57	WF4	2 × 800, 2 × 900	9	[O I] λ3727
F336W	3321/380	PC1	2 × 800, 709, 900	22	[Ne V] $\lambda\lambda$3346, 3426 and UV continuum

PLATE 4

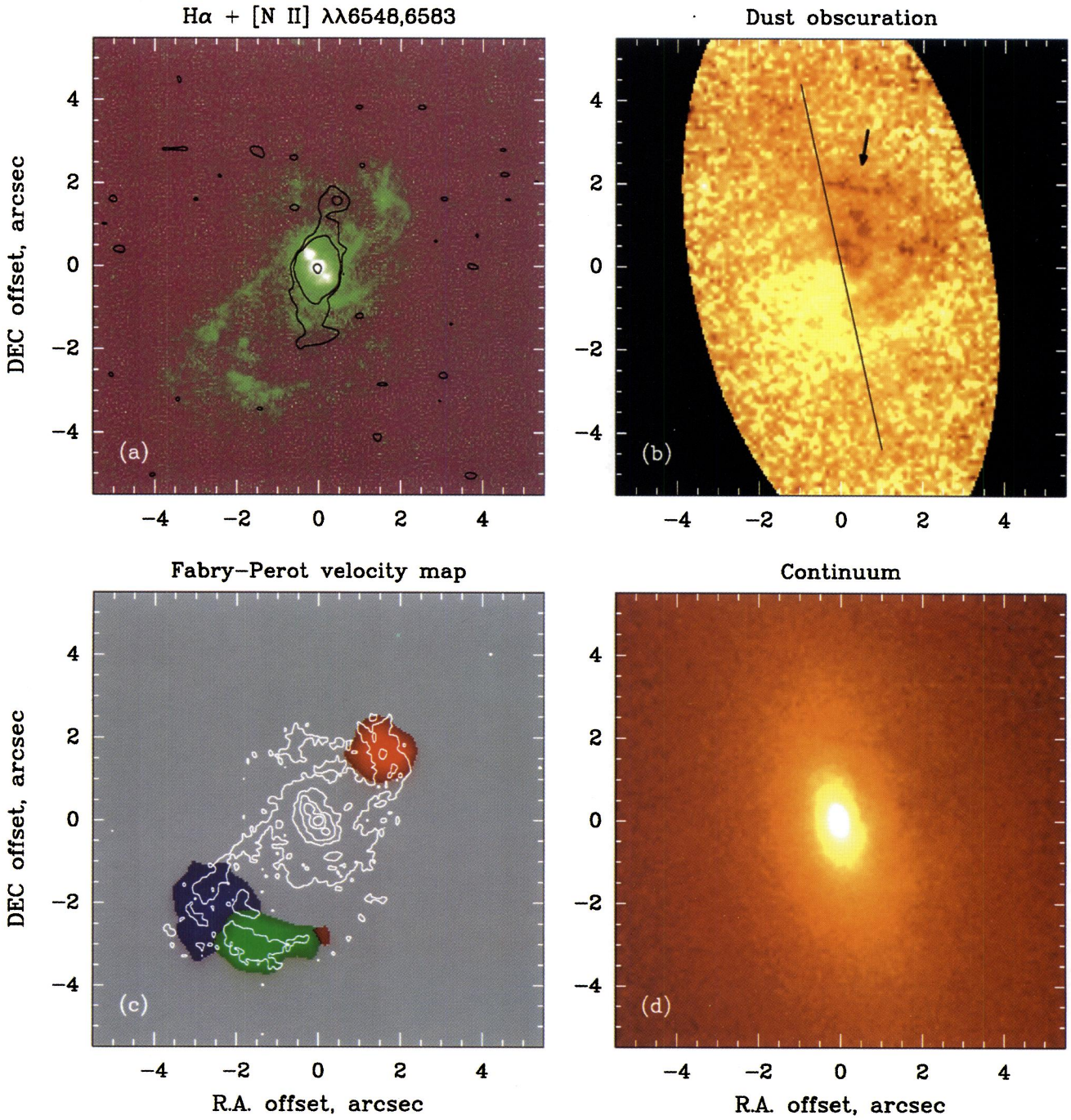

FIG. 2.—(*a*) The central 11″ of the Hα + [N II] emission-line image at the full resolution of the PC. The 6 cm VLA contours from WT94 are overplotted. The nuclear radio source has been assumed to coincide with the optical continuum peak, and contours are plotted at 0.75, 1.5, and 95% of the peak radio flux. (*b*) Map of the dust obscuration as represented by the ratio of the continuum image to a smooth, symmetric elliptical model (see § 3.2). The arrow points to the filament that we used to calculate the obscuring column density, while the line marks the galaxy major axis. (*c*) Fabry-Perot [O III] λ5007 velocity map. For clarity, velocities derived near the nucleus and outside the spiral structure are not shown. Red, green, and blue correspond to $+90$ km s^{-1}, 0 km s^{-1}, and -90 km s^{-1}, respectively, relative to the systemic velocity of the galaxy. The white contours show the continuum-subtracted Hα + [N II] emission at 5%, 10%, 15%, 25%, and 45% of the peak value of the middle nuclear knot. (*d*) Line-free continuum image (F588N). Although many of the obscuring filaments can be traced in this continuum image, they are much better outlined in the dust obscuration map of (*b*).

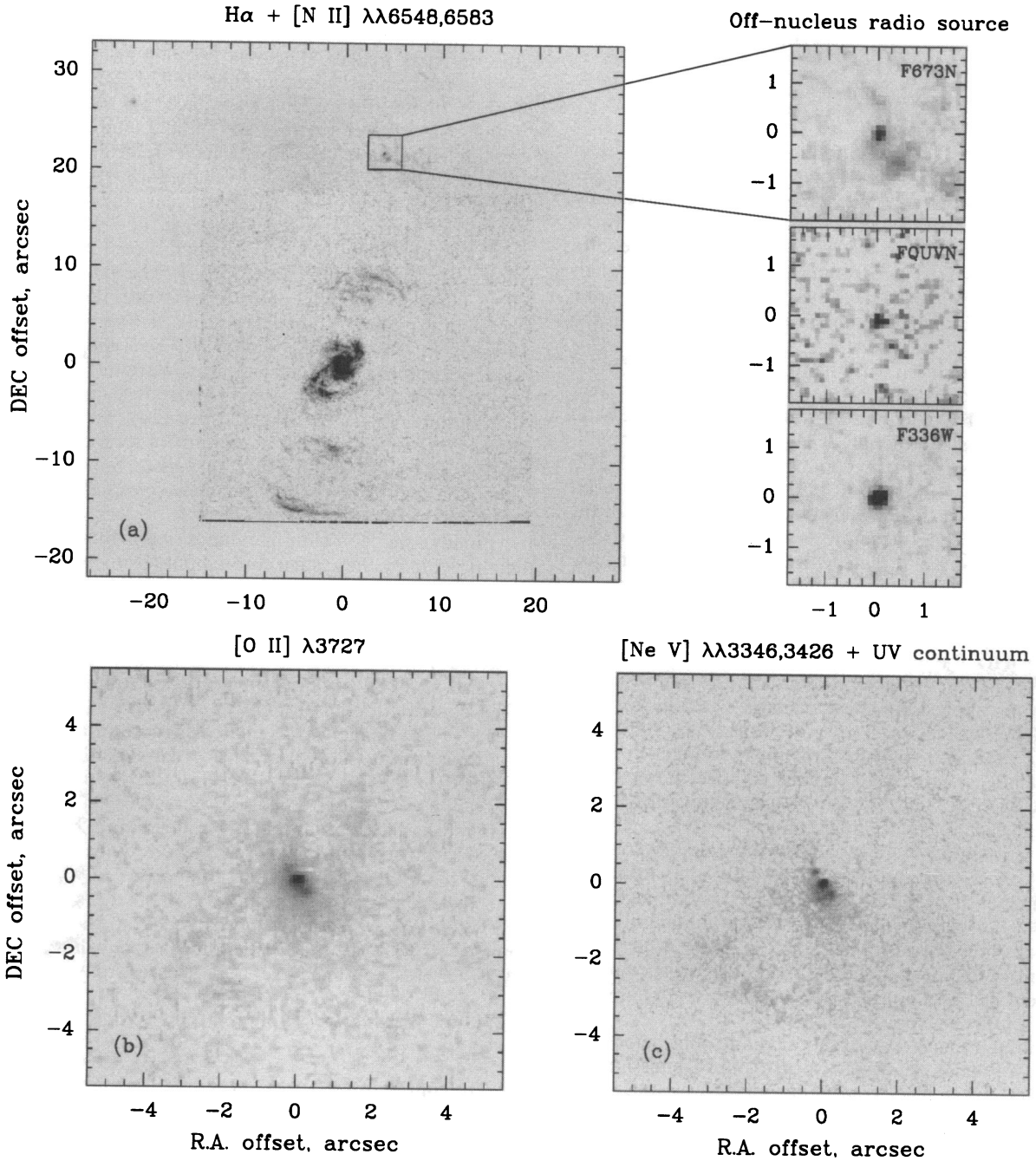

FIG. 1.—(*a*) Continuum-subtracted Hα + [N II] image of NGC 5252. The image is a mosaic of the four WFPC2 CCDs in which the outer parts of the WFPC2 field of view have been excluded. North is 1°.5 clockwise off the vertical axis. The inserts show the area around the off-nuclear radio source in three filters: F673N (mean wavelength/effective width 6733/47 Å), FQUVN (3830/57 Å), and F336W (3321/380 Å). (*b*) Continuum-subtracted [O II] λ3727 image. (*c*) Continuum-subtracted [Ne V] λλ3346, 3426 image.

images, [O II] λ3727 (Fig. 1*b*) and [Ne V] λλ3346, 3426 (Fig. 1*c*), have much lower signal-to-noise ratios and were not used to analyze the extended gaseous morphology.

3.1.1. *Gas Distribution Near the Nucleus*

Three bright knots dominate the line emission in the innermost 1″ in NGC 5252. They are aligned along P.A. ~ 35° and are embedded in fainter diffuse gas (see Figs. 1*b*, 1*c*, 2*a*, and 2*c*). The radial brightness profile of the central peak, presumably the nucleus, measures ~2 pixels (~0″.1) FWHM on PC1 and is unresolved. The clumps that bracket the nucleus have radial profiles measuring 3.2 pixels (0″.15) and 4.7 pixels (0″.21) FWHM for the northeast and southwest components, respectively, and so they are resolved. The northeast clump has a tail that extends several pixels away from the nucleus. The southwest component has a comma-shaped extension stretching several pixels to the east (see Figs. 1*c* and 2*a*). The isophotes of the fainter diffuse emission are elongated ~1″.7 (750 pc) near P.A. ~35°, aligning roughly with the three central clumps.

The two clumps that bracket the nucleus may be complexes of dense gas clouds that are exposed to ionizing radiation from the nucleus. Alternatively, they may delineate a coherent structure, such as a gaseous bar or highly inclined disk. The alignment of the nuclear clumps and the apparent association of the outer two with the ends of several extended spiral filaments (see below) are consistent with a gaseous bar that may lay in the plane of the stellar disk. If, instead, the clumps delineate a disk, the minor-to-major axis ratio $b/a \leq 0.4$–0.5 in the diffuse emission implies an inclination to the line of sight of $i \geq 60°$.

The Hα flux can be used to constrain the mass of ionized gas in the nuclear region. We measure $F(\mathrm{H}\alpha + [\mathrm{N\ II}]) = 9.1 \times 10^{-14}$ ergs cm^{-2} s^{-1} in a 1.″7 aperture centered on the brightest (middle) peak. The three colinear knots dominate this emission. Accounting for the contribution of the [N II] λλ6548, 6583 lines and using [N II] λ6583/Hα ∼ 0.5, as suggested by ground-based spectroscopy (Acosta-Pulido et al. 1995), we obtain $F(\mathrm{H}\alpha) \approx 5.7 \times 10^{-14}$ ergs cm^{-2} s^{-1}. The mass of ionized gas can be expressed as $M_{\rm gas} = CN_p m_p j(\mathrm{H}\alpha)^{-1} L(\mathrm{H}\alpha)$, where C accounts for the contribution by He, $j(\mathrm{H}\alpha)$ is the volume emissivity, and $L(\mathrm{H}\alpha)$ is the luminosity in Hα. Assuming 10% helium abundance by number, and electron temperature $T_e = 10^4$ K, the ionized mass is $M_{\rm gas} \approx 3.3 \times 10^7 F_{-14}(\mathrm{H}\alpha)/N_e\ M_\odot$, where $F_{-14}(\mathrm{H}\alpha)$ is in units of 10^{-14} ergs cm^{-2} s^{-1} and N_e is in cm^{-3}. For the observed Hα flux, and assuming an average electron density in the nuclear region of $N_e \sim 400$ cm^{-3} (Acosta-Pulido et al. 1995), we obtain $M_{\rm gas} \sim 4.7 \times 10^5\ M_\odot$.

3.1.2. *Spiral Filaments at Larger Radii*

Several filaments of Hα + [N II]–emitting gas define a tightly wound, counterclockwise spiral pattern outside the nuclear region (Fig. 2*a*). Although some filaments connect to the nuclear region, none seem to link directly to the nucleus; instead, they originate from the outer two blobs.

The spiral stretches along P.A. = 135°, roughly perpendicular to the three collinear nuclear clumps. For comparison, the axis of the ionization cone projects at P.A. = 163°. Most filaments are contained within the 74° opening angle of the ionization cone that TT89 measured from much larger scale emission-line maps. However, some (e.g., the north ridge of the southeast arm) lie outside the extrapolated edges of the sharp cone. The southeast filament, which is the brightest, extends ∼3.″5 from the nucleus and separates into many emission-line knots of size ≲0.″18 to >0.″30. Similarly, emission knots are found within other filaments. The brightest knot is located ∼2.″25 from the nucleus in P.A. = 315°, where several smaller arms intersect.

3.1.3. *Correlation with the Radio Structure*

The radio emission in the central few arcseconds of NGC 5252 (Fig. 2*a*; WT94) consists of an unresolved (≤0.″1) core, presumably associated with the true nucleus, and weak "jets" that extend ∼2″ north and south. The jets align closely with the axis of the ionization cone, P.A. = 163° ± 3°. In Figure 2*a* we have overplotted the 6 cm radio contours (WT94) on the Hα + [N II] image, assuming that the radio core coincides with the brightest Hα knot, which is also assumed to coincide with the peak of the continuum image. Although this radio-optical alignment is not warranted by absolute coordinate measurements, we believe it is correct because it puts the radio core at the expected position of the active nucleus and implies that the off-nuclear radio source coincides with a compact optical feature, as we now discuss.

A 1.9 mJy (at 6 cm) off-nuclear radio source (WT94) is located ≈22″ from the nucleus in P.A. = 351.°1; it is unresolved at wavelengths between 3.6 and 20 cm (FWHM size [3.6 cm] < 0.″10). WT94 argued that this source is associated with NGC 5252 because of its proximity to one of the emission-line arcs and to the radio jet/ionization cone axis and the low a posteriori probability of finding a background radio source at that flux level so close to the nucleus. Intriguingly, our WFPC2 images reveal a point source embedded in one of the emission-line arcs (Fig. 1 insert). This source coincides to within 1 PC1 pixel (<46 mas) with the off-nuclear radio source if the nuclear radio source is registered on the middle Hα + [N II] nuclear clump. Interpreting the off-nuclear source as a supernova in NGC 5252 is ruled out by the nonvariable radio flux (WT94). The source is detected in our F673N (Hα + [N II]), FQUVN ([O II] λ3727), and F336W (UV continuum + [Ne V] λλ3346, 3426) images but is not detected in the continuum F588N image. The radio spectrum (spectral index $\alpha \sim 0.5$, $S_\nu \sim \nu^{-\alpha}$) resembles that of a quasar, and the source appears quite blue in our images. While it is tempting to declare it a background quasar unrelated to NGC 5252, all filters in which it is detected contain emission lines at the redshift of NGC 5252. A more certain identification, therefore, must await a deep optical spectrum.

Figure 2*a* shows that the radio jets have little morphological association with the Hα + [N II] filaments. Both jets align closely with the ionization cone (P.A. = 163°) and are apparently unrelated to the general elongation of the spiral arms along P.A. = 135°. The two jets extend out to only ∼2″ radius, well inside the spiral filaments. It seems likely that the spiral pattern lies in a disk (see §§ 3.2 and 3.3) and that there is no direct interaction between the radio jets and the line-emitting gas.

3.2. *Dust in the Nuclear Region*

The visual continuum image of NGC 5252 (Fig. 2*d*; TT89) is dominated by the bulge of this S0 galaxy. Closer inspection, however, reveals an obvious asymmetry in the central few arcseconds; the northwest side of the nuclear region is fainter than the southeast side. There are also dark filaments visible on the northwest side (Fig. 2*d*). KP95 suggested that the nuclear region is extinguished by $A_V \sim 1$ mag, based on their near-infrared/optical colors. They also found a band of red material that extends ∼3 kpc roughly east-west across the nucleus. Analysis of the TT89 optical continuum images of NGC 5252 also suggests asymmetric extinction around the nucleus.

To better determine the morphology of the obscuration, we have matched a smooth axisymmetric model of the continuum brightness distribution to the observed image. We fitted elliptical isophotes to the continuum image in Figure 2*d* using the STSDAS task "ellips." The position of the nucleus was fixed after it was found that isophotes with semimajor axes of up to 120–150 PC1 pixels (5.″5–6.″8) were concentric. A symmetric model was then built from the results of the isophotal analysis by suppressing the third- and fourth-order Fourier coefficients. The model reproduces the major axis brightness profile, ellipticity, and orientation of the observed image. Then we divided the continuum image by this model. Assuming that the intrinsic stellar brightness distribution is represented by our model, this ratio maps the dust obscuration (Fig. 2*b*).

Figure 2*b* reveals a striking asymmetry in the dust distribution of the nuclear region. Obscuration is confined to a D-shape on the northwest side of a line in P.A. ∼ 15° (the

major axis of the galaxy disk) that passes through the nucleus. Many of the details in the Hα + [N II] emission-line image, in particular some of the spiral arms, can also be traced in the dust image. This is characteristic of an inclined disk of gas and dust that shadows background galaxy starlight. Some emission-line filaments can be traced farther in the dust image (i.e., outside the ionization cone), suggesting that the emitting spiral features are illuminated sectors of continuous structures that surround the nucleus. We measure a disk size of ~2″ along the straight edge of the D (P.A. = 15°) and ~2.″6 perpendicular to it. The observed morphology can be understood as two tilted, intersecting planes that are seen in projection; the other half of the D-shaped dusty disk is hidden behind the principal plane of the galaxy stellar disk and, thus, it is not visible in absorption against the starlight. The Hα + [N II] emission from the southeast side, on the other hand, does not appear to be significantly attenuated after passing through the stellar disk. The dusty disk appears to be viewed at an inclination $i \approx 40°$ to the line of sight, judging by the ratio of major to minor axes.

The obscuration in the spiral filaments on the northwest side is significant, removing up to 20%–25% of the light. The filaments appear sharp perpendicular to their lengths (both in emission and in absorption), but their widths are resolved with FWHM ranging from 0.″17 to over 0.″25 (75–110 pc). Diffuse Hα + [N II] emission is detected between the arms at a level of 2.5–4 σ above the background. There is also some hint that low-level obscuration (at a 2%–3% level) is associated with this diffuse emission, but this is model dependent.

3.3. *Kinematics and Geometry*

The Hα + [N II] image (Fig. 2*a*) suggests a rotating gas disk, so the maximum observed velocity gradient should coincide with the major axis. The extent of the spiral arms is large enough to resolve partially from the ground. Figure 2*c* shows the velocity field of the spiral arms, as mapped by an imaging Fabry-Perot (FP) spectrometer at ~30 km s^{-1} FWHM resolution (Morse et al. 1995), with contours of the Hα + [N II] emission from Figure 2*a* superposed. The velocity field is characterized using three FP images, taken at −90 km s^{-1} (blue), 0 km s^{-1} (green), and +90 km s^{-1} (red) relative to the systemic velocity of the galaxy. The nuclear region is spatially unresolved from the ground and has been masked out. Figure 2*c* shows that the northwest side is redshifted while the southeast side is blueshifted, and that the maximum velocity range is indeed measured along the major axis of the structure. In addition, a strong velocity gradient is measured along the bright southeast arm. Only the brightest parts of the spiral arms could be adequately distinguished in the ground-based observations. The velocity gradient along the southeast arm is more continuous on the scale of the seeing than suggested by Figure 2*c*.

We can speculate on the geometry of the various structures that we observe in the central regions of NGC 5252. We find evidence for three distinct planes: (1) *The principal plane of the stellar disk.* Based on an analysis of the continuum isophotes, the stellar disk lies along P.A. ~ 15° and is inclined ~60° to the line of sight. To explain the obscuration pattern in Figure 2*b*, the southeast side of the stellar disk must be the near side and the northwest side must be the far side. The stellar rotation curve observed by Held et al. (1992) shows that the stars rotate toward us in the south and away in the north. (2) *The plane of the spiral gas disk.* The projected major axis of this plane along P.A. ~ 135° is nearly perpendicular to the axis of the three collinear nuclear clumps. That several spiral filaments seem to start (or end) at the outer two nuclear clumps might indicate that these structures are physically connected. The disk is inclined ~40° to the line of sight. For trailing spiral arms, the disk is rotating clockwise on the sky and, given the kinematics (Fig. 2*c*), the northeast side projected above the major axis is the near side. The plane of the stellar disk cuts through the spiral pattern along P.A. ~ 15°, and the stars lie in front of the filaments to the southeast and behind them to the northwest. (3) *The plane of the putative torus that surrounds the central black hole.* The radio jet and the ionization cone axes are closely aligned along P.A. = 163° in NGC 5252 (WT94). In the unified model, the axes of radio jet and ionization cone are perpendicular to the nuclear torus. Therefore, the (unresolved) nuclear torus would have its projected major axis along P.A. ~73° and, if the radio jet/ionization cone axis is nearly in the plane of the sky, the nuclear torus would be edge-on. Such an orientation for the nuclear torus is broadly consistent with the east–west band of red material observed by KP95. We argue in the next paragraph that the axis of the ionization cone cannot be tilted by more than ~40° out of the plane of the sky. Under this constraint, there does not appear to be any plausible combination of inclinations and projections that would allow the three collinear nuclear clumps (possibly a bar) to be perpendicular to the radio jet/ionization cone axis (i.e., oriented in the plane of the nuclear torus). If indeed the three collinear clumps represent a small-scale bar, the geometry resembles that in NGC 5728 (Wilson et al. 1993; Shaw et al. 1993), where one of the ionization cone edges is parallel to the major axis of a nuclear stellar bar and the cone axis projects ~30° to it.

As mentioned in § 3.1.2, some of the line-emitting filaments in the spiral structure extend slightly outside the ionization bi-cone when the sharp edges of the large-scale bi-cone are extrapolated down to the nucleus.[7] Assuming that photoionization by the nucleus dominates local contributors, such as shocks, the true opening angle of the bi-cone would have to be somewhat larger than the ~75° opening angle seen on large scales. If the large-scale arcs of emission are in a plane, then this plane might be tilted relative to the axis of the ionization cone, and the arcs would intersect the cones along chords that do not indicate the true cone diameter. But the offset between the plane containing the large-scale emission arcs and the ionization cone axis cannot be too large. On the one hand, if the plane containing the arcs was tilted from the plane of the sky and the gas motions are rotational, large azimuthal velocity gradients would be seen across the arcs in disagreement with our FP observations (Morse et al. 1995). In addition, several of the arcs are close to circular (TT89), suggesting that they are seen nearly face-on. On the other hand, the ionization cone axis cannot be tilted too far out of the plane of the sky before our line of sight would fall within the cone. As the cone axis tilts farther from the plane of the arcs, the true cone opening angle must increase to intersect the arcs with the observed distribution. If we allow the opening angle to increase to ~105°, so that the outer two clumps that bracket the nucleus lie just inside the northeast/southwest cone edge and are therefore illuminated by ionizing nuclear radiation, then the cone

[7] Some of the ambiguity will be resolved when we obtain the WFPC2 [O III] λ5007 image because ionization cones are much better delineated by the high-ionization [O III] λ5007 line and especially by the [O III] λ5007/(Hα + [N II]) line ratio.

axis cannot be tilted by more than $\sim 40°$ from the plane of the sky, or our line of sight would fall within the cone. The recent discovery of a broad component to the Hα line profile of the nucleus (Osterbrock & Martel 1993; Acosta-Pulido et al. 1995) may indicate that our line of sight is fairly close to the cone edge.

3.4. *Physical Conditions in the Line-emitting Filaments*

Because the spiral filaments are resolved and we can estimate the extinction, it is possible to estimate the gaseous density and mass. The extinction in magnitudes can be expressed as $A_\lambda = -2.5 \log (I_{obs}/I_{model})$. For the best outlined filaments (e.g., the one marked by the arrow in Fig. 2*b*), we obtain $A_{5880\ Å} \approx 0^m.25$. For a standard Galactic extinction law and a normal dust-to-gas ratio $A_V \approx 5 \times 10^{-22} N_H$ (e.g., Bohlin, Savage, & Drake 1978), we obtain a neutral hydrogen column density of $N_H \approx 5 \times 10^{20}$ cm^{-2} through this filament. The lateral size of the filament is ~ 80 pc (0".18 FWHM). Assuming that the filament is a cylinder, we obtain a volume number density of $n_H \sim 2/f$ cm^{-3}, where f is the volume filling factor. We note that, although the filaments have various shapes, they all have similar A_λ and a relatively small range of observed sizes and therefore column densities.

The ionized gas density in the filaments can be estimated from the observed Hα flux. Assuming case B conditions (Osterbrock 1989), the Hα luminosity is $L(\mathrm{H}\alpha) = j(\mathrm{H}\alpha)Vf$, where V is the volume of the filament and j(Hα) is the volume emissivity of the line-emitting gas. For an electron temperature of $T_e \sim 10^4$ K, $j(\mathrm{H}\alpha) = 3.6 \times 10^{-25} n_p n_e$. In the same area used to estimate obscuration in the previous paragraph (see Fig. 2*b*), we measure $F(\mathrm{H}\alpha) \approx 6 \times 10^{-17}$ ergs cm^{-2} s^{-1} from a region of ~ 80 pc (0".18) centered on the filament. The corresponding number density of ionized gas is then $n_p \sim 5/(f)^{1/2}$ cm^{-3}. Some other filaments and knots have up to 10 times higher Hα surface brightness, tripling this density estimate.

Our two estimates of the filament's density, based on absorption and on Hα emission, agree within a factor of a few, an insignificant difference because of uncertainties in the underlying assumptions and because the obscuration is more likely to be associated with the neutral gas (if any), whereas Hα traces the ionized fraction. Our most important result is that the *HST* images suggest very low densities if the filaments are filled uniformly with gas. This is consistent with the ground-based spectroscopy (Acosta-Pulido et al. 1995; Morse et al. 1995), which indicates electron densities of a few hundred cm^{-3} from the [S II] λλ6716, 6731 doublet ratios at the nucleus and in the low-density limit elsewhere.

We thank J. Holtzman, J. Hester, J. Biretta, and W. Sparks for useful discussions and suggestions regarding WFPC2 calibrations. We also thank T. Statler for his insights on the dynamics of galaxy cores. Support for this work was provided by NASA through grants NAGW-3268, GO-5426.01-93A, and GO-5426.02-93A.

REFERENCES

Acosta-Pulido, J. P., Vila-Vilaro, B., Pérez-Fournon, I., Wilson, A. S., & Tsvetanov, Z. I. 1995, ApJ, submitted
Antonucci, R. R. J. 1993, ARA&A, 31, 473
Bohlin, R. C., Savage, B. D., & Drake, J. F. 1978, ApJ, 224, 132
Heathcote, S., Reipurth, B., Morse, J. A., Bally, J., Hartigan, P., Schwartz, R. D., & Stone, J. M. 1995, in preparation
Held, E. V., Capaccioli, M., & Cappellaro, E. 1992, in Testing the AGN Paradigm, ed. S. Holt, S. Neff, & C. M. Urry (New York: AIP), 613
Holtzman, J. A., et al. 1995a, PASP, 107, 156
———. 1995b, PASP, submitted
Huchra, J., & Burg, R. 1992, ApJ, 393, 90
Kotilainen, J. K., & Prieto, M. A. 1995, A&A, 295, 646 (KP95)
Morse, J. A., et al. 1995, in preparation
Osterbrock, D. E. 1989, Astrophysics of Gaseous Nebule and Active Galactic Nuclei (Mill Valley: University Science Books)
Osterbrock, D. E., & Martel, A. 1993, ApJ, 414, 552
Prieto, M. A., & Freudling, W. 1993, ApJ, 418, 668
Shaw, M. A., Combes, F., Axon, D. J., & Wright, G. S. 1993, A&A, 273, 21
Tadhunter, C., & Tsvetanov, Z. 1989, Nature, 341, 422 (TT89)
Wilson, A. S., Braatz, J. A., Heckman, T. M., Krolik, J. H., & Miley, G. K. 1993, ApJ, 419, L61
Wilson, A. S., & Tsvetanov, Z. I. 1994, AJ, 107, 1227 (WT94)